

Supporting Information

Fully Efficient Direct Yb-to-Er Energy Transfer at Molecular Level in a Near-Infrared Emitting Heterometallic Trinuclear Quinolinolato Complex

*Flavia Artizzu, Francesco Quochi, Luciano Marchiò, Elisa Sessini, Michele Saba, Angela Serpe,
Andrea Mura, Maria Laura Mercuri, Giovanni Bongiovanni and Paola Deplano*

Experimental Section

General

All the reagents and solvents were purchased from Aldrich and used without further purification. Electronic UV-Vis-NIR: Diffuse reflectance (DR) on KBr pellets and Teflon films and absorption spectra were collected using a Varian Cary 5 and a Perkin Elmer Lambda 950 spectrophotometers. Vibrational FTIR spectra on KBr (MIR, 4000-400 cm^{-1}) and polyethylene (FIR, 400-50 cm^{-1}) pellets were collected using a Bruker Equinox 55 spectrophotometer. Elemental analysis data were collected using a Carlo Erba mod. EA1108 CHNS analyzer. Mass spectra were obtained with a Micromass ZMD spectrometer operating in positive ionization mode.

Syntheses

Synthesis of 1: Few drops of NH_3 28% up to a final concentration of $2.0 \times 10^{-2} \text{ mol dm}^{-3}$ ($\text{pH} \cong 10$) were added to a mixture of 8-hydroxy-quinoline (0.145 g, 1 mmol) in H_2O (100 mL) under mixing. After 30 min a water solution of $\text{YbCl}_3 \cdot 6\text{H}_2\text{O}$ (0.129 g, 0.33 mmol) was added to the above mixture which is allowed to react for 2 days until the white solid due to the unreacted ligand disappears. A yellow precipitate is formed, collected by filtration, washed with water, NaOH 0.1 M, water, and dried in oven at 120°C (almost quantitative yield). Analytical results are in agreement with $\text{Yb}_3\text{Q}_9 \cdot 3\text{H}_2\text{O}$ formulation. CHN Found (Calculated for $\text{C}_{81}\text{H}_{60}\text{Yb}_3\text{N}_9\text{O}_{12}$): C% 52.18(52.01), H% 3.35(3.23), N% 6.82(6.74). The solid was then dissolved in warm CH_3CN , the solvent was roto-evaporated to incipient precipitation and after several days yellow microcrystals of Yb_3Q_9 were obtained (yield 46%). CHN Found (Calculated for $\text{C}_{81}\text{H}_{54}\text{Yb}_3\text{N}_9\text{O}_9 \cdot \text{CH}_3\text{CN}$): C% 54.07 (53.67); H% 3.20 (3.09); N% 7.56 (7.54). FT-IR, cm^{-1} : 3047 m, 1601 m, 1571 s, 1498 vs, 1466 vs, 1424 mw, 1383 s, 1318 s, 1276 m, 1231 m, 1174 w, 1109 vs, 1035 w, 907 w, 823 m, 804 m, 788 m, 732 s, 648 m, 607 m, 592 w; 571 w, 504 m, 490 m, 458 w, 419 mw, 397 m, 384 m, 376 m, 353 m, 335 vw, 326 w, 315 vw, 303 w, 290 w, 280 m, 266 w, 253 m, 247 m, 226 m, 203 m, 177 m, 151 ms, 140 m, 132 m, 121 m, 101m 90 m 80 mw, 74 mw, 57 mw. UV-Vis-NIR absorption, nm, [$\text{mol}^{-1} \text{ dm}^3 \text{ cm}^{-1}$], DMSO: 340[$1.43 \cdot 10^4$], 379[$2.09 \cdot 10^4$], 977 ($^2\text{F}_{5/2} \rightarrow ^2\text{F}_{7/2}$) [20]; Diffuse reflectance, nm: 262, 344, 385; 928, 952, 979 ($^2\text{F}_{7/2} \rightarrow ^2\text{F}_{5/2}$), 1147(3vC-H), 1683 (2vC-H). ESI-Mass ($\text{CH}_3\text{CN}/\text{CH}_3\text{OH}$ 3/1), m/z: 1671.87 [Yb_3Q_8^+].

Synthesis of 2: Synthesis was carried out following the same procedure described for **1**, by adding to a solution containing 1 mmol of the ligand, a mixture of 0.22 mmol of $\text{YbCl}_3 \cdot 6\text{H}_2\text{O}$ and 0.11 mmol of $\text{ErCl}_3 \cdot 6\text{H}_2\text{O}$ in water. A yellow precipitate is formed, collected by filtration, washed with water, NaOH 0.1 M, water, and dried in oven at 120°C (almost quantitative yield). CHN Found (Calculated for $\text{C}_{81}\text{H}_{54}\text{Yb}_2\text{ErN}_9\text{O}_9 \cdot 3\text{H}_2\text{O}$): C% 52.25(52.17), H% 3.38(3.24), N% 6.87(6.76). Yellow microcrystals were obtained after recrystallization from CH_3CN (yield 38%). CHN Found (Calculated for $\text{C}_{81}\text{H}_{54}\text{Yb}_2\text{ErN}_9\text{O}_9 \cdot 3\text{H}_2\text{O}$): FT-IR, cm^{-1} : 3047 m, 1601 m, 1571 s, 1498 vs, 1466 vs, 1424 mw, 1383 s, 1318 s, 1276 m, 1231 m, 1174 w, 1109 vs, 1035 w, 907 w, 823 m, 804 m, 788 m, 732 s, 648 m, 607 m, 592 w; 571 w, 504 m, 489 m, 458 w, 419 mw, 397 m, 384 m, 377 m, 353 m, 335 vw, 326 w, 315 vw, 303 w, 289 w, 280 m, 267 w, 253 m, 247 m, 226 m, 203 m, 177 m, 151 ms, 140 m, 132 m, 121 m, 105 m, 101 m, 89 m, 80 mw, 74 mw, 57 mw. UV-Vis-NIR absorption, nm, [$\text{mol}^{-1} \text{ dm}^3 \text{ cm}^{-1}$], DMSO: 340[$1.43 \cdot 10^4$], 379[$2.10 \cdot 10^4$], 977 ($^2\text{F}_{5/2} \rightarrow ^2\text{F}_{7/2}$) [20], 1504 [3.5]; Diffuse reflectance, nm: 262, 344, 385; 928, 952, 979 ($^2\text{F}_{7/2} \rightarrow ^2\text{F}_{5/2}$), 1147(3vC-H), 1506, 1533 ($^4\text{I}_{13/2} \rightarrow ^4\text{I}_{15/2}$), 1683 (2vC-H). ESI-Mass ($\text{CH}_3\text{CN}/\text{CH}_3\text{OH}$ 3/1), m/z: 1666.54 [$\text{Yb}_2\text{ErQ}_8^+$].

SEM-EDX and X-ray powder diffraction

SEM-EDX analyses were performed with a FEI Dual Beam Nova NanoLab 600i equipped with a EDAX Genesis microanalyzer.

Wide-angle XRD-patterns on microcrystalline powder samples were recorded with a Panalytical Empyrean diffractometer equipped with a graphite monochromator and a X'Celerator linear detector. The scans were collected within the range $5\text{-}90^\circ$ (2 θ) using $\text{Cu K}\alpha$ radiation.

Photoluminescence measurements

Photoluminescence (PL) was excited at 392 nm wavelength by the frequency-doubled output pulses of a regenerative Ti:Sapphire amplifier (Quantronix INTEGRA C) running at repetition frequency of 1 kHz. Vis PL decay transients were captured by a streak camera (Hamamatsu C5680) equipped with an imaging spectrometer (Acton SpectraPro

2300i). NIR PL was wavelength dispersed by an Acton SpectraPro 2300i spectrometer; optical spectra and decay transients were detected using, respectively, an InGaAs CCD (Andor iDus) and an InGas photomultiplier (Hamamatsu H10330A-75) connected to a 1 GHz digitizing oscilloscope (Tektronik TDS 5104). In order to minimize nonlinear effects possibly taking place in doubly excited complexes, photoexcitation fluences were kept below the level of 0.1 excitation per complex per laser pulse in all experiments. According to Poissonian statistics, an average excitation level of 0.1 yields a fractional population of doubly excited complexes of ca. 5×10^{-3} . CW visible PL spectra were recorded using a Horiba Jobin-Yvon FluoroMax-4 spectrofluorimeter.

Vibrational Spectroscopy

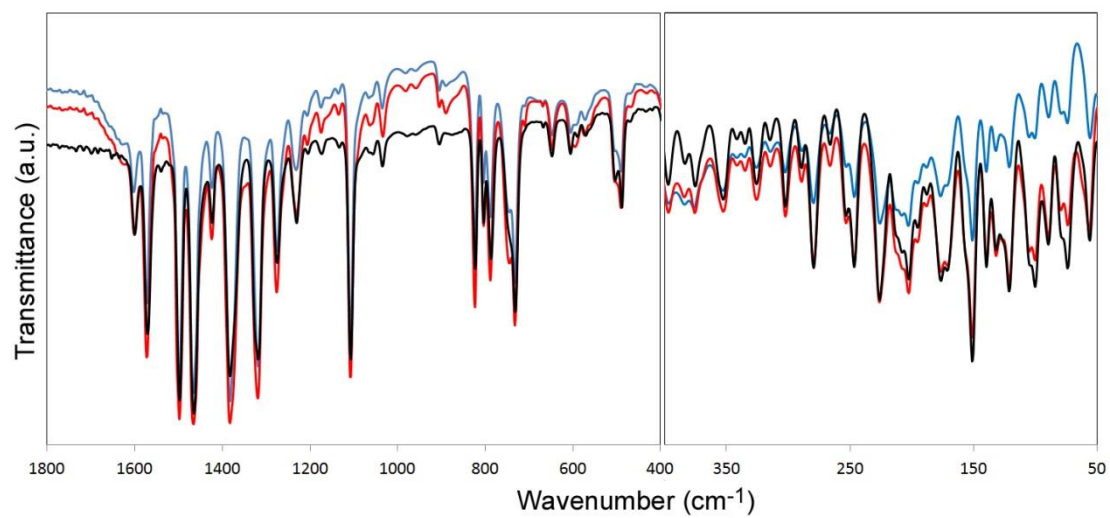


Figure S11. FT-IR spectra of **1** (red), **2** (blue) and Er₃Q₉ (black) in the MIR (4000-400 cm⁻¹, KBr pellet) and in the FIR (400-50 cm⁻¹, polyethylene pellet).

Powder X-ray diffraction

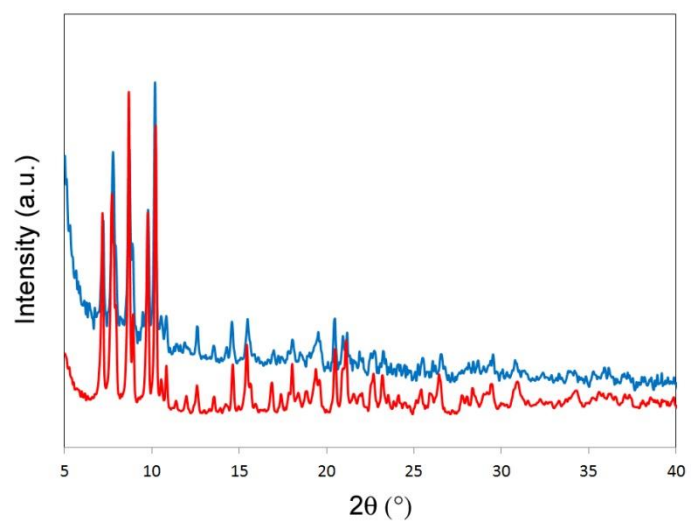


Figure S12. Powder XRD in the 5-40° angle (2θ) of **1** (red) and **2** (blue).

SEM-EDX analysis

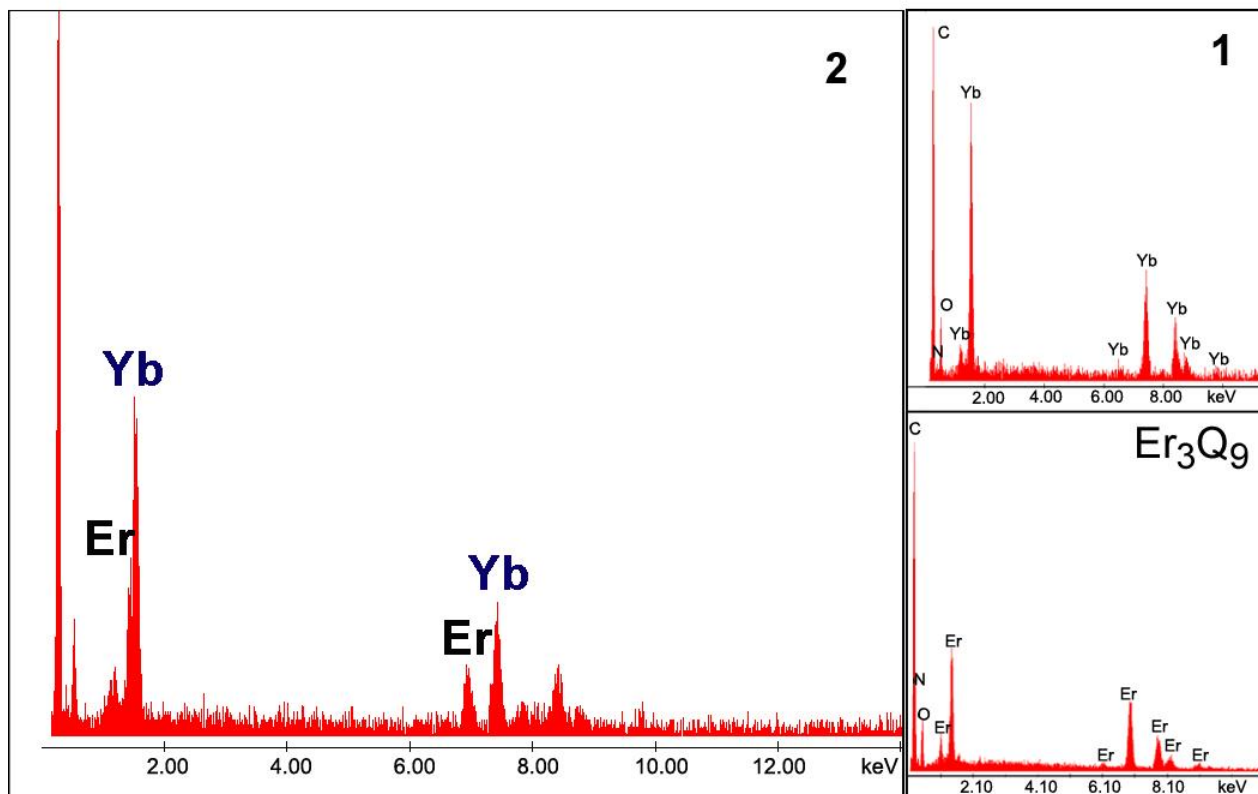


Figure S13. X-ray energy dispersive spectra for 2, 1 and Er₃Q₉.

Table S11. EDX analysis results for 2.

EDAX Element Table	ZAF Normalized :	Quantification, Default	Standardless,				
Element,	Wt	%,	At	%,	K-Ratio,	Z,	A,
ErL,	33.40,	34.16,	0.3309,	1.0030,	0.9879,		1
YbL,	66.60,	65.84,	0.6684,	0.9984,	1.0052,		1
Total,	100.000,		100				
Element,	Net	Inte.,	Bkgd	Inte.,	Inte.	Error,	P/B
ErL,	17.70,	4.10,	6.43,	4.32			
YbL,	33.10,	4.50,	4.38,	7.36			

Measurements were performed on several batches of 2, and EDX data were acquired on at least three spots per each sample, yielding very good reproducibility.

ESI-Mass analysis

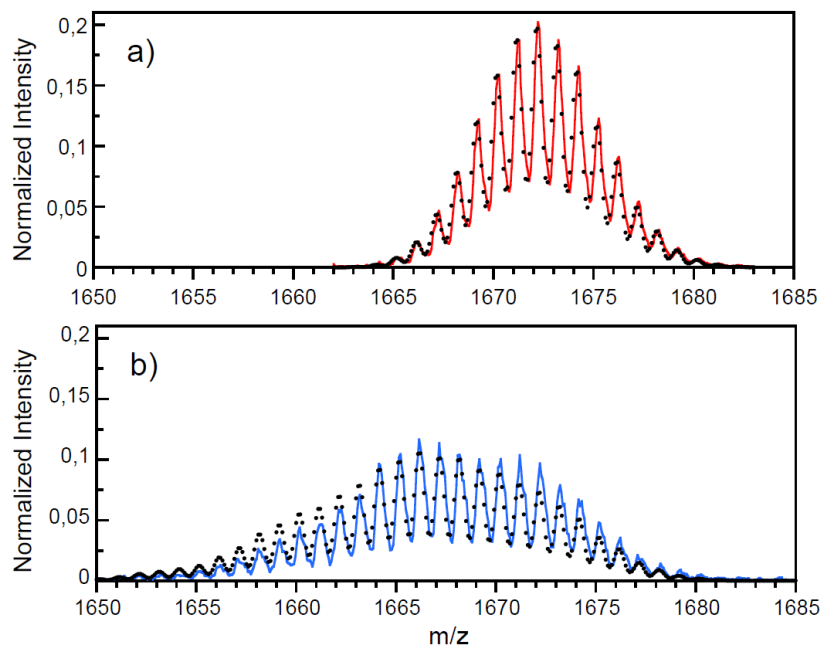


Figure SI4. Normalized mass spectra of **1** (a) and **2** (b) showing the isotopic distribution. Dots represent calculated distributions for Yb_3Q_9 (a) and for a statistical mixture of Yb_2ErQ_9 (44%), YbEr_2Q_9 (22%), Yb_3Q_9 (30%) and Er_3Q_9 (4%) (b), assuming that the $[(\text{Er-Yb})\text{Q}_8]^+$ fragmentation yield is independent of the Er and Yb number of occurrences in the fragment.

Erbium absorption cross-section

For accurate evaluation of erbium absorption cross-section at about 1.5 μm , anhydrous dimethylsulfoxide solvent was used to limit the amount of water in the solution and the concentration of the complex was pushed up to the solubility limit (10^{-2} M). The spectrum of **2** (1 cm cuvette pathlength) was then compared to that of an equimolar solution of **1** in which an absorption feature appears in the region 1400-1620 nm (see Figure S15). The intensity of this feature does not change upon dilution of **1** and is also observed in the spectrum of the pure solvent. Therefore it can be attributed to weak vibrational harmonic bands of solvent or small amount of water contamination. The corrected spectrum of **2** at about 1.5 μm was then obtained by subtracting the spectrum of **1**. This method was also used for Er_3Q_9 (results published in ref. 28). The same absorption cross-section per erbium atom was found for **2** and Er_3Q_9 ($\sigma_{\text{Er}}[{}^4\text{I}_{13/2} \leftarrow {}^4\text{I}_{15/2}] = 1.0 \cdot 10^{-20} \text{ cm}^2$).

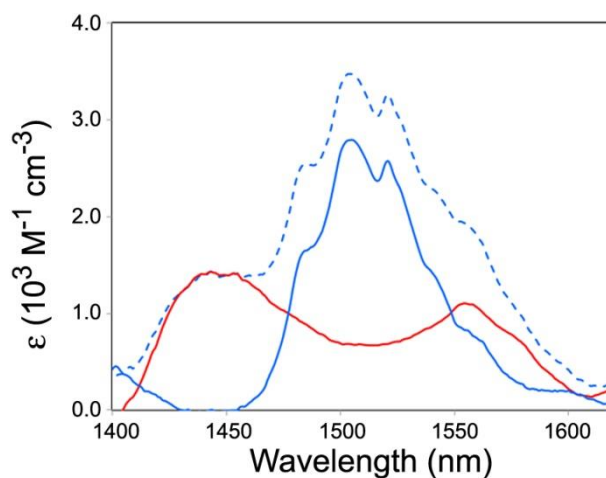


Figure S15. Absorption spectra of **1** (red) and **2** (dashed blue line) in the 1400-1620 nm region. The continuous blue line represents the erbium ${}^4\text{I}_{13/2} \leftarrow {}^4\text{I}_{15/2}$ absorption band corrected for solvent effects (see text).

Ligand-centered optical properties

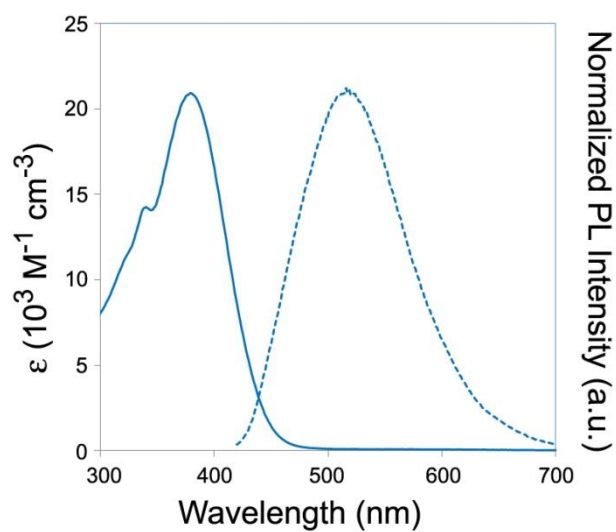


Figure SI6. Ligand absorption and normalized PL spectra for **2** in DMSO solution. Complex **1** shows the same spectral features in the visible region.

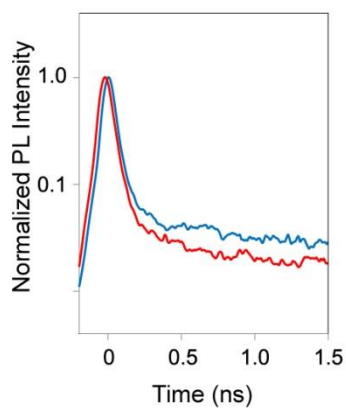
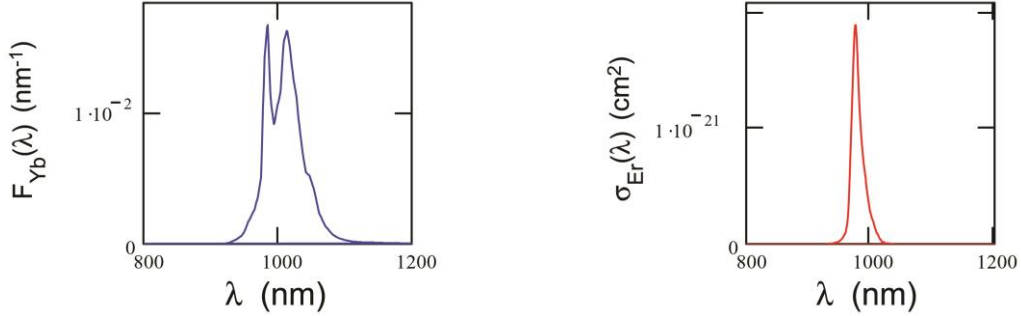


Figure SI7. Normalized visible emission transients for **1** (red) and **2** (blue) excited at 392 nm. The ultrafast (resolution limited) initial decay of the visible emission is traced back to intersystem crossing depopulating the photoexcited ligand-centered singlet states.

Förster's model

$$J = \int F_{Yb}(\lambda) \sigma_{Er}(\lambda) \lambda^4 d\lambda$$

Overlap integral between the emission band of the donor ($F_{Yb}(\lambda)$) and the absorption band of the acceptor ($\sigma_{Er}(\lambda)$)



$$J \cdot 10^{35} = 3.36 \cdot 10^{-3} \text{ cm}^6$$

Donor-Acceptor overlap integral

$$R_0 = \sqrt[6]{\frac{9\kappa_j^2}{128\pi^5 n^4} \int F_{Yb}(\lambda) \sigma_{Er}(\lambda) \lambda^4 d\lambda}$$

where κ^2 ($= 0.667$) is a geometrical factor that depends on the relative orientation between the donor-acceptor transition dipoles, and n is the refractive index of the medium (1.478 for DMSO)

$$R_0 = 1.01 \cdot 10^{-7} \text{ cm}$$

Förster's radius

$$k_{RET} = \frac{1}{\tau_{RET}} = \frac{1}{\tau_{Yb}} \left(\frac{R_0}{R_{Yb-Er}} \right)^6$$

Förster's energy transfer rate constant ($k_{RET \text{ YbEr}}$) and time constant ($\tau_{RET \text{ YbEr}}$). τ_{Yb} ($= 10 \mu\text{s}$) is the decay time of the donor (Yb) in the absence of the acceptor (Er), R_{Yb-Er} ($= 3.5 \text{ \AA}$) is the donor-acceptor distance.

$$\tau_{RET \text{ YbEr}} = 1.71 \cdot 10^{-8} \text{ s}$$

Förster's energy transfer time constant (Model)

$$\eta_{RET} = \frac{1}{1 + \frac{\tau_{RET}}{\tau_{Yb}}}$$

$$\eta_{RET \text{ YbEr}} = 0.998$$

Förster's energy transfer efficiency (Model)

$$\tau_{RET} = \frac{1}{1/\tau_{YbEr} - 1/\tau_{Yb}}$$

where τ_{YbEr} ($= 50 \cdot 10^{-9} \text{ s}$) represents the lifetime of Yb feeding the $\text{Er } ^4I_{11/2}$ level

$$\tau_{RET \text{ YbEr}} = 5.03 \cdot 10^{-8} \text{ s}$$

Energy transfer time constant (Experimental)

$$\eta_{RET} = \frac{1}{1 + \frac{\tau_{RET}}{\tau_{Yb}}}$$

$$\eta_{RET \text{ YbEr}} = 0.995$$

Energy transfer efficiency (Experimental)